Transition-State Spectroscopy of the Photoinduced Ca + CH 3 F Reaction. 3. Reaction Following the Local Excitation to Ca(4s3d 1 D)

ARTICLE *in* THE JOURNAL OF PHYSICAL CHEMISTRY A · MARCH 2008

Impact Factor: 2.69 · DOI: 10.1021/jp077664g · Source: PubMed

7 AUTHORS, INCLUDING:

Eric Gloaguen
French National Centre for Scientific Research
64 PUBLICATIONS **424** CITATIONS
SEE PROFILE

Cristina Sanz Sanz
Universidad Autónoma de Madrid
34 PUBLICATIONS **362** CITATIONS
SEE PROFILE

B. Soep
Atomic Energy and Alternative Energies Com…
155 PUBLICATIONS **2,250** CITATIONS
SEE PROFILE

Octavio Roncero
Spanish National Research Council
142 PUBLICATIONS **2,821** CITATIONS
SEE PROFILE

Transition-State Spectroscopy of the Photoinduced Ca + CH_3F Reaction. 3. Reaction Following the Local Excitation to Ca(4s3d ^{1}D)

E. Gloaguen, C. Sanz Sanz,† M. Collier, M.-A. Gaveau, B. Soep, O. Roncero,† and J.-M. Mestdagh*

Laboratoire Francis Perrin (CNRS-URA-2453), DSM/IRAMIS/Service des Photons, Atomes et Molécules, C.E.A. Saclay, F-91191 Gif-sur-Yvette cedex, France

Received: September 24, 2007; In Final Form: December 3, 2007

The Ca* + $CH_3F \rightarrow CaF^* + CH_3$ reaction was studied both experimentally and theoretically. The reaction was photoinduced in Ca···CH_3F complexes, which were illuminated by a tunable laser in the range 18 000−24 000 cm^{-1}. The absorption band that leads to the reaction extends between 19 000 and 23 000 cm^{-1}. It is formed of three broad overlapping structures corresponding to the excitation of different electronic states of the complex. The two structures of lowest energy were considered in detail. They are associated with two series of respectively 2 and 3 molecular states correlating to Ca(4s3d ^{1}D) + CH_3F at infinite separation between Ca and CH_3F. The assignment of these structures to specific electronic transitions of the complex stemmed from theoretical calculations where the Ca···CH_3F complex is described by a linear Ca−F−C backbone. 2D potential energy surfaces were calculated by associating a pseudopotential description of the [Ca^{2+}] and [F^{7+}] cores, a core polarization operator on calcium, an extensive Gaussian basis, and a treatment of the electronic problem at the CI-MRCI level. All the excited levels correlating to the 4s^2 ^{1}S, 4s3d ^{1}D, and 4s4p ^{1}P levels of Ca in the Ca + CH_3F channel were documented in a calculation that explored the rearrangement channels where either Ca + CH_3F or CaF + CH_3 are formed. Then, wavepacket calculations on the 2D-PES's allowed one to simulate the absorption spectrum of the complex, in an approximation where the various electronic states of the complex are not coupled together. The assignment above stemmed from this. The second outcome of the calculation was that whatever the excited level of the complex that is considered, the reaction has to proceed through energy barriers. The electronic excitation of the complex on the red side of the absorption band does not seem to deposit enough energy in the system to overcome these barriers (even the lowest one) or to stimulate tunneling reactions. An alternative reaction mechanism involving a transfer to triplet PES's is proposed.

1. Introduction

The reaction

$$Ca + CH_3F \rightarrow CaF + CH_3 \qquad \Delta H = -80\ \text{kJ/mol} = -0.83\ \text{eV} \quad (1)$$

is exothermic. It is blocked by a barrier that cannot be overcome when the reactants are in the ground electronic state and "frozen" within a cold Ca···CH_3F complex. The electronic excitation of the complex using a laser turns on the reaction and electronically excited CaF is observed:[1,2]

$$Ca\cdots CH_3F \xrightarrow{h\nu} CaF^* + CH_3 \quad (2)$$

The harpoon mechanism is often invoked to describe oxidation reactions of electronically excited metal atoms by molecular reactants.[3] Under its simplest form, it reduces the dynamics of the reaction to a one-dimensional path across the transition state (TS) of the reaction, where an electron jumps suddenly from the metal atom to the molecular reactant. Accordingly, the system experiences sequentially a 1D approach of the metal toward the molecule and after the electron jump, a 1D dissociation. Two different coordinates are at play in the reaction, which do not act simultaneously.

The dynamics of reaction 2 is interesting because it is prototypical of situations that are not adequately described by this very simple picture. The molecular reactant, CH_3F, needs to be deformed for attaching an extra electron, hence making at least two coordinates active simultaneously. Other representative examples are the Li + HF, CH_3F reactions reported by the group of Polanyi[4,5] and the Ba + CH_3F reaction studied extensively in the groups of Ureña[6−16] and Radloff.[17−21]

The present paper is the third in a series dedicated to reaction 2. The earlier works in this series have identified two excitation bands in the Ca···FCH_3 complex that lead to reaction 2.[1,2] They are extending quite far on each side of the resonance line of free calcium (23 652 cm^{-1}). For a large part, the red band (called band A in ref 2) is associated with the excitation of molecular states that correlate to Ca(4s3d ^{1}D) at large separation between Ca and FCH_3, whereas the blue band (band B) is due to molecular states correlating to Ca(4s4p ^{1}P). The theoretical approach developed in ref 2 has suggested that the reaction mechanism associated with the excitation to band B involves a multidimensional dynamics with no clear separation in the TS region between the approach of the metal atom and the

* Corresponding author. E-mail: jean-michel.mestdagh@cea.fr.
† Instituto de Física Fundamental, C.S.I.C., Serrano 123, 28006 Madrid, Spain.

10.1021/jp077664g CCC: $40.75
Published on Web 01/31/2008

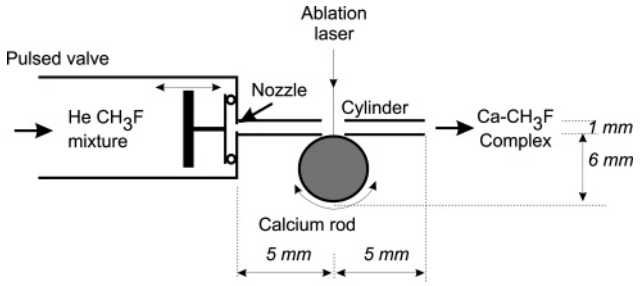

Figure 1. Scheme of the laser evaporation source.

deformation of the molecular reactant. The reaction mechanism associated with the excitation to band A has not been examined yet.

The present work is both experimental and theoretical. It examines the mechanism of reaction 2 when the Ca···FCH_3 complex is excited to band A (between 19 000 and 23 500 cm^{-1}). On the experimental side, it is a continuation of a previous one where the electronically excited product of reaction 2, CaF, was monitored as a function of the wavelength of the laser that turns on the reaction.[2] Complementary information is provided here on the lifetime of the excited complex by monitoring the complex itself. Indeed, if the complex is long-lived, it can be ionized by a nanosecond laser and can be detected as the $CaCH_3F^+$ ion:

$$Ca\cdots CH_3F \xrightarrow{h\nu} (Ca\cdots CH_3F)^* \xrightarrow{h\nu'} (CaCH_3F)^+ \qquad (3)$$

The possible competition with the dissociation channel is examined also.

$$Ca\cdots CH_3F \xrightarrow{h\nu} Ca^* + CH_3F \qquad (4)$$

On the theoretical side, the present work simulates the absorption spectrum of the complex over the excitation range 19 000−23 500 cm^{-1} explored experimentally. It simulates also the excited-state dynamics of the system by a wavepacket propagation on a two-dimensional model of the potential energy surfaces (2D-PES) that explores two exit valleys: the dissociation as Ca* + CH_3F (process 4) and the reaction forming CaF (process 2). These two valleys are called hereafter the *entrance* and the *reaction* valleys, respectively.

2. Experiment

The experimental apparatus combines a pulsed supersonic beam carrying the 1:1 Ca···CH_3F complex, nanosecond lasers and a time-of-flight mass spectrometer (TOF-MS). A first laser photoexcites the complexes whereas a second one ionizes the products that are mass analyzed subsequently using the TOF-MS. Action spectra are recorded by monitoring the ion signals at the desired mass while scanning the photoexcitation laser.

2.1. Beam Source. Cold van der Waals complexes Ca···CH_3F are generated using the laser evaporation source schemed in Figure 1. It is composed of a piezoelectric pulsed valve, a nozzle of 0.5 mm diameter, and a cylinder of 1 mm diameter and 10 mm length in which a rotating rod of calcium is ablated by the 532 nm doubled output of a YAG laser. A mixture of 8% CH_3F in helium is pushed through the nozzle and mixed in the cylinder with the Ca vapor created by the laser ablation. The beam expansion is constrained by the cylinder. It produces cold Ca···CH_3F complexes but as usual in laser evaporation sources, the desired compound is mixed with other species: CaF molecules, clusters of Ca and CaF plus various mixed clusters of Ca, CaF and CH_3F (see section 4.1). Careful adjustments of the operating conditions are reported in section 4.1 for the 1:1 Ca···CH_3F complexes to be present in sufficient quantity. Note, these conditions do not guaranty that the complex are very cold.

The molecular beam is collimated by a 2 mm skimmer on entering the chamber where the reaction dynamics experiments are performed.

2.2. Lasers. A pulsed tuneable dye laser (Lambdaphysic LPD 3000) is pumped by either the 532 or 355 nm outputs of a nanosecond YAG laser. Two kinds of experiment are performed under two arrangement of the laser:

•***Beam characterization*** in a single laser arrangement: the dye laser is frequency-doubled, delivering tunable light between 207 and 240 nm.

•***Reaction dynamics experiments*** in a pump/probe arrangement: the dye laser is used as the "pump" to excite the complex over the spectral range 421−535 nm; part of the 355 nm light of the YAG laser is delayed by 5 ns and used as the "probe" to detect the reaction products by ionization.

No reference signal exists to normalize the reaction dynamics signal with respect to the amount of complexes present in the beam. Besides stochastic fluctuations that cannot be corrected, this amount has also a periodic variation due to the rotation of the calcium rod, hence modulating the reaction dynamics signal accordingly. Because the action spectra are obtained by continuously scanning the "pump" laser, this produces an oscillation in the measured spectra, which is removed numerically by cutting the corresponding Fourier component.

3. Calculations

3.1. Two-Dimensional Potential Energy Surfaces (2D-PES). The calculations are performed using the MOLPRO ab initio package.[22] They aim to describe the excited-state potential energy surfaces (PES) in both valleys where either Ca approaches CH_3F (entrance valley) or CaF approaches CH_3 (reaction valley). A collinear Ca−F−C geometry forming a plane of symmetry with one of the C−H bonds is chosen to explore the PES as a function of the Ca−F and F−C distances. Doing so, offers the advantage of dealing with a two-dimensional grid with a minimum in the ground-state potential that is close to the slightly bent equilibrium geometry found for the ground-state Ca···FCH_3 complex in ref 2. With this choice, the complex belongs to the C_s symmetry group and its electronic states are of either $^1A'$ or $^1A''$ symmetry. Six $^1A'$ and three $^1A''$ are calculated. They correspond to the states that correlate with the $4s^2$ ^1S, 4s3d ^1D, and 4s4p ^1P atomic states of Ca upon dissociation of the Ca···FCH_3 complex as Ca + CH_3F. The adiabatic correlation of the calculated states to the electronic states of Ca and CaF in the entrance and reaction valleys are shown in the top and bottom part of Table 1, respectively.

The present calculations of the excited PES's is performed with two objectives: (i) a correct description of the vertical transition energies from the equilibrium geometry of the ground-state complex; (ii) a correct description of the energy barriers and minima in both the entrance and reaction valleys to provide information on the reaction mechanism and its competition with dissociation as Ca + CH_3F.

To fulfill the first requirement, the basis sets, effective potentials, and core-polarization operator successfully applied in ref 2 are used again in the present work. The second requirement is more challenging: the system is quite large and has a very strong ionic character in the reaction valley (the static dipole of CaF is 3.07 Debye[23]) whereas no such character exists

TABLE 1: Calculated and Experimental Energies (in cm^{-1}) at Large Separation between Ca and CH_3F (Top Table) and between CaF and CH_3 (Bottom Table)[a]

state	R_{CF}	R_{CaF}	calculation	experiment	asymptote
			Dissociation: $Ca + CH_3F$		
$1^1A'$	2.613	20.0	0.0	0.0	$Ca(4s^2\ ^1S) + CH_3F$
$2^1A'$	2.613	20.0	21406	21850[33]	$Ca(4s3d\ ^1D) + CH_3F$
$3^1A'$	2.613	20.0	21418		
$4^1A'$	2.613	20.0	21425		
$2^1A''$	2.613	20.0	21419		
$1^1A''$	2.613	20.0	21406		
$5^1A'$	2.613	20.0	23283	23652[33]	$Ca(4s4p\ ^1P) + CH_3F$
$6^1A'$	2.613	20.0	23315		
$3^1A''$	2.613	20.0	23283		
			Reaction: $CaF + CH_3$		
$1^1A'$	11.0	3.7	0.0	0.0	$CaF(X^2\Sigma^+) + CH_3$
$2^1A'$	11.0	3.7	16143	16530[40]	$CaF(A^2\Pi) + CH_3$
$1^1A''$	11.0	3.7	16150		
$3^1A'$	11.0	3.7	18625	18841[30]	$CaF(B^2\Sigma^+) + CH_3$
$4^1A'$	11.0	3.7	22394	21544[41]	$CaF(B'^2\Delta) + CH_3$
$2^1A''$	11.0	3.7	22459		
$5^1A'$	11.0	3.7	30182	30159[42]	$CaF(D^2\Sigma^+) + CH_3$
$6^1A'$	11.0	3.7		30216[42]	$CaF(C^2\Pi) + CH_3$
$3^1A''$	11.0	3.7	31303		

[a] The experimental values correspond to the electronic excitation energies of either Ca or CaF. The theoretical ones are taken from the IC-MRCI calculation of the PES at the C−F and Ca−F distances (in au) marked in the table.

in the entrance valley, $Ca + CH_3F$. Because we look for excited electronic states correlating in both valleys, crossings and important configuration changes are encountered when switching from one valley to the other. Hence, the convergence of the calculations is often a challenge.

An appropriate compromise between computation time and accuracy is found by performing the excited-state calculations at the IC-MRCI level (Internally Contracted-MultiReference Configuration Interaction, namely the CI command in MOLPRO) using the reference wavefunctions provided by a state-averaged MCSCF calculation (MultiConfiguration Self-Consistent Field, command MULTI of MOLPRO). Special attention is given to the orbitals that are included in the MCSCF calculation to reproduce satisfactorily the degeneracy of the states correlating with the excited states of Ca and CaF in the entrance and reaction valleys. This is achieved by first computing the Ca and CH_3F moieties separately. Then, the orbitals of both systems are associated to create a set of orbitals for the whole system $CaFCH_3$. The latter set is sorted with all the occupied orbitals of CH_3F at first and then the s, d, and p orbitals of Ca. The core orbitals of the full system include inner electrons of CH_3F and no electron of Ca. Different active spaces were attempted until both asymptotes, the entrance as $Ca + CH_3F$ and the reaction as $CaF + CH_3$, are well reproduced after improving the electron−electron correlation at the IC-MRCI level. The best compromise is found with an active space composed of 4 core ($3^1A'$, $1^1A''$), 3 closed ($2^1A'$, $1^1A''$), and 13 active orbitals ($10^1A'$, $3^1A''$).

The relevance of the IC-MRCI calculation to describe the excited states of Ca and CaF is satisfactory, as shown in Table 1. The relative energy of degenerated levels fall always within 32 cm^{-1}, except for the levels corresponding to the $CaF(B'^2\Delta) + CH_3$ asymptote that are separated by 115 cm^{-1}. The absolute energies of the excited levels are underestimated by less than 450 cm^{-1} for calcium and for the A, B and D states of CaF. The energy of the $CaF(B'^2\Delta)$ state is overestimated by 882 cm^{-1} whereas that of the highest calculated state, $CaF(C\ ^2\Pi)$, is overestimated by 1090 cm^{-1}. Note that for convergence problems the $6^1A'$ state is not documented in the reaction valley.

The 2D PES's are provided by the IC-MRCI calculations by varying the Ca−F and F−C distances in the linear Ca−F−C backbone of the $CaCH_3F$ system. They are mapped by a 20 × 18 rectangular grid, where the Ca−F distance is set to 3.0, 3.2, 3.3, 3.5, 3.7, 3.8, 4.0, 4.2, 4.4, 4.6, 4.8, 5.0, 6.0, 7.0, 8.0, 10.0, 12.0, 15.0, 18.0, 20.0 bohr and the F−C distance to 1.8, 2.113, 2.313, 2.413, 2.613, 3.0, 3.5, 4.0, 4.5, 5.0, 5.5, 6.0, 6.5, 7.0, 7.5, 8.0, 12.0, 15.0 bohr. A 2D spline interpolation of these data for each state is used to generate the 2D PES's of the first six $^1A'$ and three $^1A''$ states of the $Ca-F-CH_3$ system.[24]

3.2. Simulation of the Absorption Spectrum. The absorption spectrum of the $Ca\cdots FCH_3$ complex is simulated in five steps: (i) parametrization of the $CaFCH_3$ system, (ii) determination of the wavefunction describing the complex prior to the photon absorption, (iii) simulation of the initial wavepacket after vertical electronic excitation of the ground-state complex, (iv) propagation of the wavepacket in each excited state, and (v) simulation of the absorption spectrum itself. Details of the specific calculations performed at each step are provided in the next paragraphs.

(i) Parametrization of the $CaFCH_3$ System. The bound-state and wavepacket calculations are performed assuming that the CH_3 subunit is a pseudo atom, *X*, of mass 15.0235 amu. Hence, the full $CaFCH_3$ system is reduced to the triatomic, Ca−F−X. It is described by standard Jacobi coordinates *r*, *R*, γ: *r* is the F−X internuclear vector; *R* is the vector joining the FX center-of-mass to the Ca atom; γ is the angle between these two vectors. The 2D PES's calculated in the previous section correspond to a linear Ca−F−C backbone of the $CaFCH_3$ (now Ca−F−X) system. To fit the 2D calculation into the 3D description provided by the Jacobi coordinate system, it is assumed that the 3D PES's are isotropic with respect to the γ angle. Hence, the angular part describing the FX rotation in the full Hamiltonian is restricted to the zero angular momentum ($j = 0$ in eq 1 of ref 25).

(ii) Bound States of the Electronic Ground State. We shall see in section 5.1 that the ground electronic state of the Ca−F−X system has a van der Waals minimum along the $Ca + CH_3F$ valley, implying that bound states exist in this region of the $1^1A'$ PES. The energy and the wavefunction associated with these states are calculated, diagonalizing the Hamiltonian defined above on a set of 10 × 15 numerical basis functions. The latter are obtained, solving the a 1-dimensional Schrödinger equation along the Jacobi coordinate *r* (or *R*) with the interaction potential in the Hamiltonian frozen at the equilibrium configuration of the other coordinate *R* (or *r*). Details can be found elsewhere.[26] The corresponding ground vibrational level in the van der Waals minimum of Ca−F−X describes the $Ca\cdots FCH_3$ complex prior to the laser excitation. The associated wavefunction Ψ_g is used in the next paragraph.

(iii) Initial Wavepacket after Vertical Excitation of the Ground-State Complex. The laser excitation of the ground-state complex is simulated by projecting the wavefunction Ψ_g on each electronically excited state of the CaFX system. The procedure is fully explained as eq (5−10) in ref 27. In the present case, the transition dipole moment is assumed to be constant as a function of the Jacobi coordinates *r* and *R* and equal to 1 for all excited states. Hence, the initial wave packet $\Psi_e(t=0)$ in each excited electronic state "e" is simply proportional to the wavefunction Ψ_g mentioned in the previous paragraph.

(iv) Wavepacket Dynamics Calculations. The initial wavepackets $\Psi_e(t=0)$ obtained above are propagated in time using the Chebyshev propagator on a two-dimensional grid formed

by 256 × 512 points that sample the radial Jacobi coordinates in the range: $0.4 \leq r \leq 9$ Å and $0.75 \leq R \leq 20$ Å. The time step of the calculation is 1 fs. No nonadiabatic coupling between PES's is introduced in the present work. Hence, the present calculation describes the adiabatic evolution of the Ca−F−X system in each excited PES. Finally, the wave packet is absorbed at the edge of the grids to avoid artificial reflection and aliasing processes. The flux in these asymptotic regions is analyzed in both the entrance and reaction channels, hence documenting the branching ratio between dissociation as the Ca + CH_3F and reaction as CaF + CH_3. More details of the calculation method are given elsewhere.[28]

(v) Simulation of the Absorption Spectrum. The wavepacket propagation at short times reflects the evolution of the electronically excited system in the vibrational levels that are accessible from the ground-state complex. Hence, the Fourier transform of the autocorrelation function $c(t) = \langle \Psi_e(t=0) | \Psi_e(t) \rangle$ of the wavepacket between time t and time zero provides the absorption spectrum toward a specific excited state of the complex. When such calculations are performed, the autocorrelation functions are multiplied by an exponential damping function, giving a Lorentzian profile of 10 cm^{-1} width to the absorption peaks (this corresponds to a 265 fs lifetime of the complex). The full absorption spectrum of the complex is obtained after summation of the individual absorption spectra.

The individual absorption spectra obtained by this method can have contributions both from the bound states and from the dissociative channels of the corresponding electronic state. Except for the 6A′ state, the absorption peaks to the other excited states of the complex all correspond to bound states with respect to both the adiabatic and adiabatic reaction channels. This is due in the latter case to the presence of a high barrier along the reaction paths that blocks the reaction although it is exothermic. Hence, the same kind of calculation as that performed in the ground state to get the bound vibrational levels has been used here to get the bound vibrational levels of the excited states. This allows us to doublecheck the wavepacket calculation and more importantly to clarify the origin of the peaks that appear in the simulated absorption spectra.

4. Experimental Results

4.1. Characterization of the Molecular Beam. When the laser is tuned to 212.5 nm (47 060 cm^{-1}), the various species present in the molecular beam are ionized directly, in particular the desired Ca···FCH_3 complexes, which lead to the $CaCH_3F^+$ ion signal. The latter parent ion is optimized by adjusting the intensity and focus of the vaporization laser, the backing pressure of the He/CH_3F gas mixture and the delays between the valve opening and the laser pulses for the evaporation and the ionization. The mass spectrum recorded under the best operating conditions is shown in Figure 2. The experimental results reported below were recorded under these conditions. A large $CaCH_3F^+$ ion signal appears with about the same height as a CaF^+ peak due to the direct ionization of CaF molecules carried by the beam. The other peaks are much less intense. Because the operating conditions provide the desired complex in a mixture with other species, care will be taken in the following to determine which of the observed signals document the dynamics of the Ca···FCH_3 complex.

4.2. Ionization Energetics of the Ca···FCH_3 Complex. When the laser is tuned over the range 207−240 nm, a threshold for detecting the $CaCH_3F^+$ ion is found at 236.6 ± 1.0 nm, indicating that the ionization energy of the Ca···CH_3F complex is 5.24 ± 0.02 eV. This value is used to locate the $(Ca\cdots FCH_3)^+$ ion with respect to the neutral complex in the energetics of the $CaCH_3F$ system shown in Figure 3.

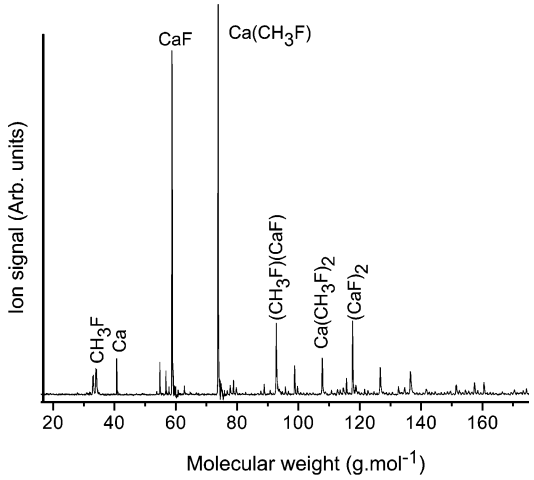

Figure 2. Mass spectrum recorded for a 212.5 nm ionization, after optimization of the beam source conditions.

When the laser is tuned above the ionization threshold, the $CaCH_3F^+$ ion is observed up to the high-energy limit of the scanning range, 207 nm, corresponding to 0.75 eV above the threshold. This observation is consistent with the calculation by Schwarz and co-workers that a barrier blocks the exothermic reaction channel $Ca^+\cdots FCH_3 \rightarrow CaF^+ + CH_3$.[29]

4.3. Action Spectra. The pump laser is tuned in the range 421−535 nm. The ionization laser that probes the $CaCH_3F$ system is at 355 nm. The energetics shown in Figure 3 show which excited levels of Ca and CaF are energetically accessible after the pump step and which ions are expected after the probe: $CaCH_3F^+$ from the ionization of the electronically excited complex, Ca^+ from the ionization of Ca(4s3d ^{1}D) and CaF^+ from that of CaF($B^2\Sigma^+$, $B'^2\Delta$). Of these ions, only CaF^+ and $CaCH_3F^+$ ions are observed experimentally.

The spectra recorded when monitoring the CaF^+ and $CaCH_3F^+$ ions are shown in Figure 4a,b, respectively.

We examine Figure 4a at first. The corresponding spectrum consists of a broad band with smooth structures extending between 445 and 520 nm, and two sharp peaks at 531 and 515 nm. Because the Ca···FCH_3 complex is not the only species present in the beam (see Figure 2), this spectrum may not be entirely due to Ca···FCH_3. The two sharp peaks arise actually from the R2PI detection of free CaF molecules that are present in the beam. Their wavelength indeed is that of the CaF($B^2\Sigma^+$-(v'=0,1) ← X $^2\Sigma^+$(v''=0)) transitions, the first step in the R2PI detection of free CaF.[30] To assign the broad band in the spectrum of Figure 4a, several time-of-flight profiles of CaF^+ are shown in Figure 5 whether the pump laser is tuned to the band or to the peaks. The TOF profiles are much broader in the former case than in the later. This is the indication that the detected molecules are produced by an exothermic process, which give them a random extra velocity as would be the case when CaF is formed in reaction 2. In contrast, the CaF molecules that already exist as free molecules in the beam have the beam velocity as unique velocity component and the TOF profile of the peak corresponding two their R2PI detection is narrow.

$CH_3F\cdots CaF$ and $(CaF)_2$ clusters also appear in Figure 2 as small components of the beam. It could be argued that the CaF signals exhibiting broad TOF profiles could arise from the dissociation of these clusters. However, it has been checked that the recoil energies deduced from the TOF profiles are not

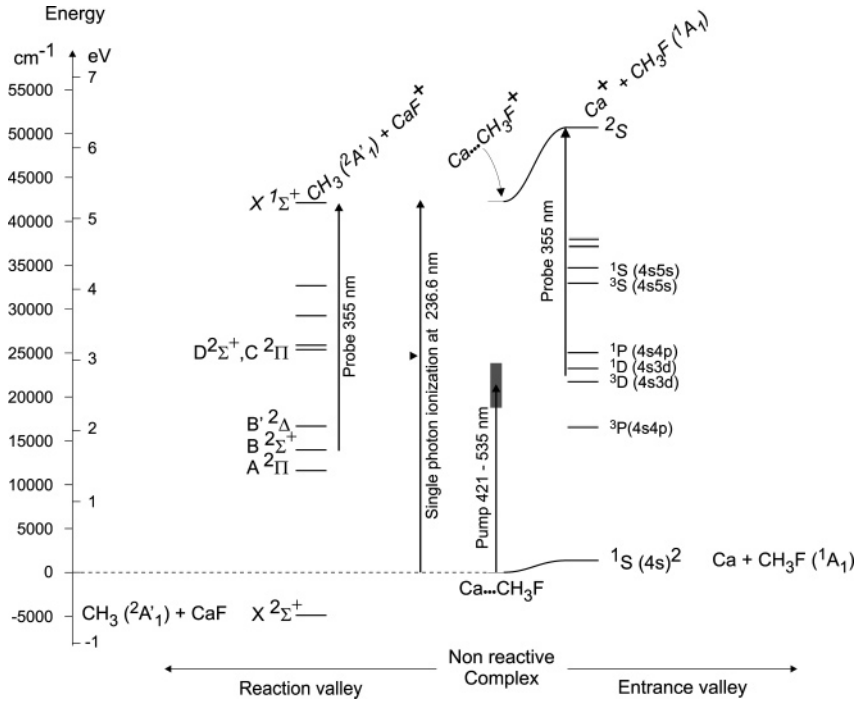

Figure 3. Energetics of the Ca + CH_3F (right side of the figure) and CaF + CH_3 (left side) system. The energies used to construct the figure are taken from refs 31, 32, 43, 44, and 29 and from the present work. Photon wavelengths are indicated where needed.

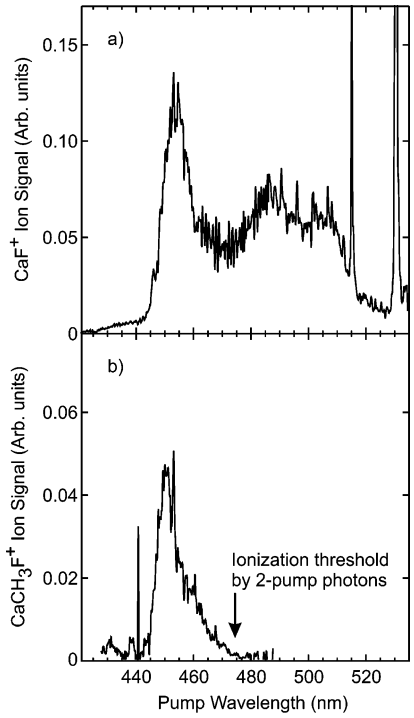

Figure 4. (a) Top panel: action spectrum measured under the pump−probe scheme I while monitoring the CaF^+ ion signal. The narrow lines at 515 and 531 nm are not relevant of the action spectrum (see the text for details). (b) Bottom panel: action spectrum measured while monitoring the $CaCH_3F^+$ ion signal. It corresponds to a R2PI detection of the Ca···CH_3F complexes by the sole pump laser (see the text for details). Note that the signal in this panel is multiplied by a factor 50 with respect to that in the top panel.

consistent with the binding energy of these clusters, expectedly larger than 0.1 eV. Hence, we consider that the broad band in Figure 4a reflects essentially the action spectrum of reaction 2 when photoinduced into Ca···FCH_3 complexes by the pump laser. However, a small contribution of larger complexes (Ca···$(CH_3F)_2$ complexes, for example) is not excluded, which may broaden the structures observed in the action spectrum.

Similarly, the signal reported in Figure 4b can be assigned unambiguously to Ca···CH_3F complexes and documents Process 3. This stems from observing the identical blue threshold of the action spectra in Figures 4a and 4b, an indication that it corresponds to the blue limit of the same absorption band of Ca···CH_3F.

A final comment must be made. The observation of CaF^+ ion signal required that both the pump and the probe lasers were present. As expected, the action spectrum reaction 2 that is shown in Figure 4a refers to a two color pump−probe scheme, with the pump tuned in the range 421−535 nm and the probe at fixed wavelength (355 nm) with a 5 ns delay. In contrast only the pump laser needed to be present for observing the $CaCH_3F^+$ ion signal. Hence the action spectrum of process 3 shown in Figure 4b is actually a resonance enhanced 2-photon ionization process (R2PI) where the pump laser acts alone, both to excite the complex and to ionize it ($\nu' = \nu$ in process 3). The fact that no two color pump−probe signal is observed contains an information on the lifetime of the electronically excited complex that is discussed later. For convenience, we call this spectrum an "action spectrum", using quotation marks to make the point.

5. Calculation Results

5.1. 2D PES's. Contour plots of the ground and excited states PES's of the Ca−F−CH_3 system are shown in Figures 6 and 7, respectively. In each surface except $6^1A'$, the bottom of the entrance valley (which corresponds to the Ca + CH_3F asymptote, parallel to the vertical axis in the figures) is fairly flat with a weak van der Waals minimum that is almost not visible at the scale of the figure. The Ca−F distance is about 4.5 au at the van der Waals minimum. In each PES, a significant barrier isolates this valley from the reaction valley corresponding to the formation of CaF + CH_3 (parallel to the horizontal axis).

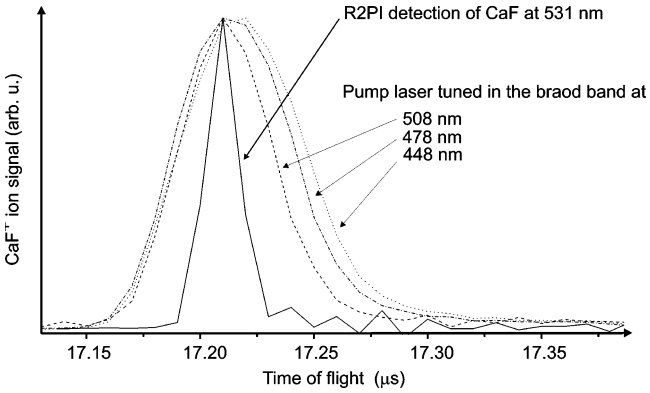

Figure 5. Profile of the CaF^+ mass peak recorded using the TOF-MS at four wavelengths of the pump laser. Three wavelengths are taken along the structured band of the action spectrum shown in Figure 4 (top panel) whereas the fourth one corresponds to one of the R2PI detection peak of CaF. The mass peaks are normalized with respect to their intensity to make their width easier to compare.

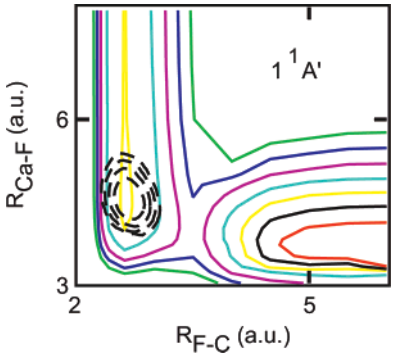

Figure 6. Ground PES of Ca−F−CH_3 provided by the IC-MRCI calculation in the collinear geometry of the Ca−F−C backbone. The vertical and horizontal scales are the Ca−F and F−C distances, describing the entrance and reaction valleys, respectively. The zero of energy corresponds to the asymptotic energy at large separation in the entrance valley. The potential contours are separated by 3×1000 cm^{-1} with the largest energy contour corresponding to $+12 \times 1000$ cm^{-1}. The density of probability associated with the ground vibrational state in the entrance valley is shown as dashed lines with contours differing by 1 order of magnitude from one to the other.

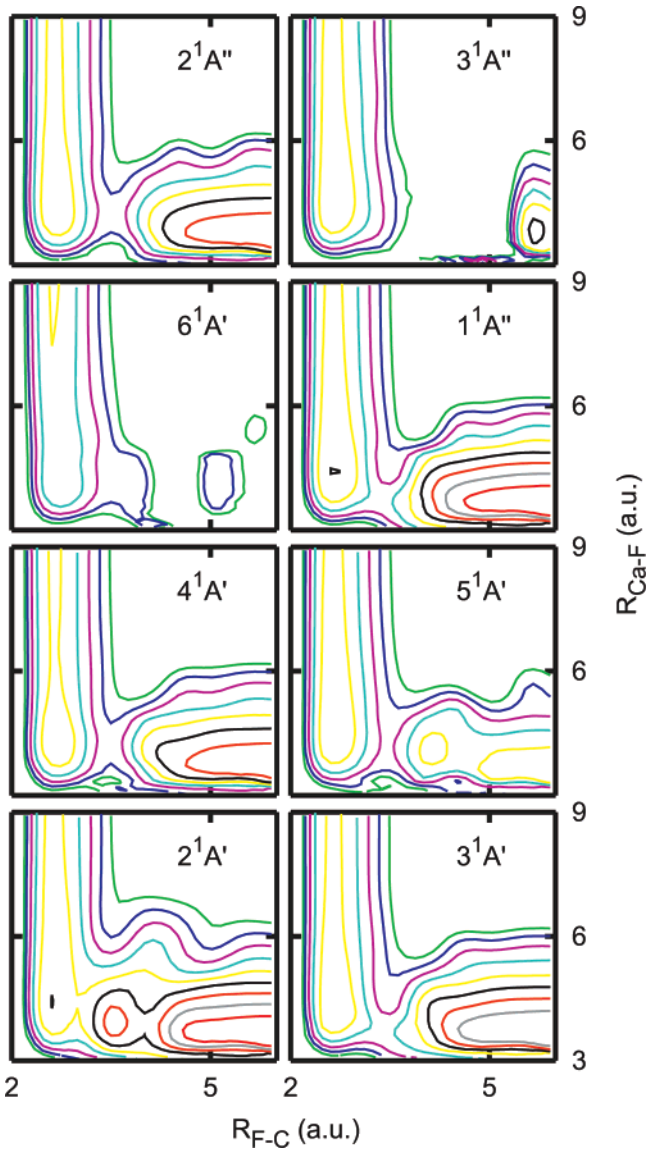

Figure 7. Same caption as Figure 6 for the excited electronic states of Ca−F−CH_3. No vibrational wavefunction is shown in this figure.

The stationary points corresponding to the van der Waals minimum and the reaction barrier of each surface are listed in Table 2. The location of the van der Waals minima is about the same whatever the PES, except for the $6^1A'$ PES where no such minimum exists. The latter surface is repulsive at large Ca−F separation and presents a suspended well at closer distance, due to an anticrossing with an upper excited state (see ref 2, where this state is examined extensively). The height (8−9000 cm^{-1}) and location of the reaction barriers are similar for all the states with the exception of the first excited state, $2^1A'$, where the barrier height is much lower, 1355 cm^{-1}.

5.2. Reaction Path. Figure 8 is a cut through the 2D PES's when following the minimum energy path from Ca + CH_3F to CaF + CH_3 in each PES. The corresponding energy profile is shown along a "reaction coordinate" defined as the difference between the Ca−F and C−F distances, subtracting a constant to set the "reaction coordinate" to zero at the van der Waals minimum of the ground PES $1^1A'$. Positive values of the reactive coordinate describe the entrance valley Ca + CH_3F whereas negative values define the reaction valley CaF + CH_3.

Nine curves correlating adiabatically to the Ca($4s^2$ ^1S), Ca(4s3d ^1D), and Ca(4s4p ^1P) asymptotes at infinite separation between Ca and CH_3F appear in Figure 8. The curves at positive values of the reaction coordinate are close to those reported in Figure 6 of ref 2 (note that the horizontal scale is not the same in each work). Following each curve in Figure 8 from right to left allows one to switch from Ca + CH_3F to CaF + CH_3. As observed in the previous section, a van der Waals minimum is met first, then a reaction barrier and finally a nonmonotonic exothermic path to the reaction. One of these profiles has a much lower barrier than the others.

The reaction exothermicity for forming the ground state of CaF + CH_3 is calculated to 1.1 eV, and it is 0.83 eV from the experiment.[31,32] Again, such agreement must be considered as satisfactory, given the difficulty of the calculation and the precision of the measurements.

5.3. Ground Electronic State: PES, Wavefunction, and Vibrational Frequencies. The depth of the van der Waals minimum at the right side of the reaction barrier is 731 cm^{-1} in the ground-state PES (see Figures 6 and 8 and Table 2). A larger depth of 850 cm^{-1} has been calculated in ref 2. In this former work, special attention was given to accurately calculate this well: the optimization was not restricted to a collinear geometry of the Ca−F−C backbone; the calculation was at the

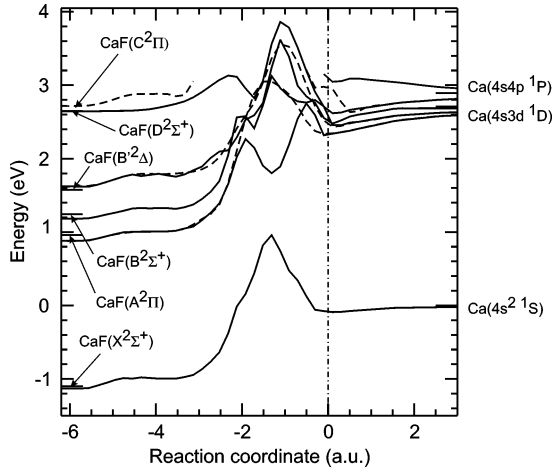

Figure 8. Calculated electronic energies at the IC-MRCI level along the reaction coordinate defined in the text. For clarity, the ground-state products CH_3F and CH_3 are skipped from the labels showing asymptotic energies in the entrance (right-hand side of the figure) and reaction valleys (left-hand side), respectively. The full and dashed curves refer to A′ and A″ states, respectively.

TABLE 2: Energies (in cm^{-1}) Provided by the IC-MRCI Calculation at the Stationary Points of the PES's of $CaFCH_3$[a]

state	R_{CF}	R_{CaF}	energy relative to the asymptote	asymptote
			Van der Waals well	
$1^1A'$	2.613	4.6	−731	Ca(4s^2 ^{1}S) + CH_3F
$2^1A'$	2.613	4.4	−2576	Ca(4s3d ^{1}D) + CH_3F
$3^1A'$	2.613	4.2	−1787	Ca(4s3d ^{1}D) + CH_3F
$4^1A'$	2.613	4.4	−1639	Ca(4s3d ^{1}D) + CH_3F
$5^1A'$	2.613	4.4	−2045	Ca(4s4p ^{1}P) + CH_3F
$6^1A'$	2.613	4.4	no van der Waals well	Ca(4s4p ^{1}P) + CH_3F
$1^1A''$	2.613	4.4	−2539	Ca(4s3d ^{1}D) + CH_3F
$2^1A''$	2.613	4.4	−1665	Ca(4s3d ^{1}D) + CH_3F
$3^1A''$	2.613	4.4	−2022	Ca(4s4p ^{1}P) + CH_3F
			Reaction Barrier	
$1^1A'$	3.4	3.7	9193	Ca(4s^2 ^{1}S) + CH_3F
$2^1A'$	3.0	3.7	1355	Ca(4s3d ^{1}D) + CH_3F
$3^1A'$	3.4	3.7	8120	Ca(4s3d ^{1}D) + CH_3F
$4^1A'$	3.4	3.7	8585	Ca(4s3d ^{1}D) + CH_3F
$5^1A'$	3.4	3.7	7774	Ca(4s4p ^{1}P) + CH_3F
$6^1A'$	3.4	3.7	9349	Ca(4s4p ^{1}P) + CH_3F
$1^1A''$	3.4	3.7	8549	Ca(4s3d ^{1}D) + CH_3F
$2^1A''$	3.4	3.7	9762	Ca(4s3d ^{1}D) + CH_3F
$3^1A''$	4.0	3.7	9057	Ca(4s4p ^{1}P) + CH_3F

[a] The Ca−F−C backbone is linear. The C−F and Ca−F distances (in au) that locate the stationary points are given in the table.

CCSD(T) level and included a correction for the Basis Set Superposition Error (BSSE). The depth of 850 cm^{-1} is thus believed to be more accurate than the present calculation. Nevertheless, the agreement between both calculations is striking. Both values are close, within experimental errors, to the value of 1400 ± 400 cm^{-1} that could be deduced from thresholds considerations on the stability of the Ca···FCH_3 complex in an experiment where another absorption band of the complex is explored (work in progress).

The wavefunction Ψ_g that is associated with the ground vibrational state of the ground electronic state is shown in Figure 6 as a contourplot of the probability density. It defines the Franck−Condon region from which the laser excitation proceeds. Finally, approximate vibrational frequencies can be deduced from the wavepacket calculation for the ground

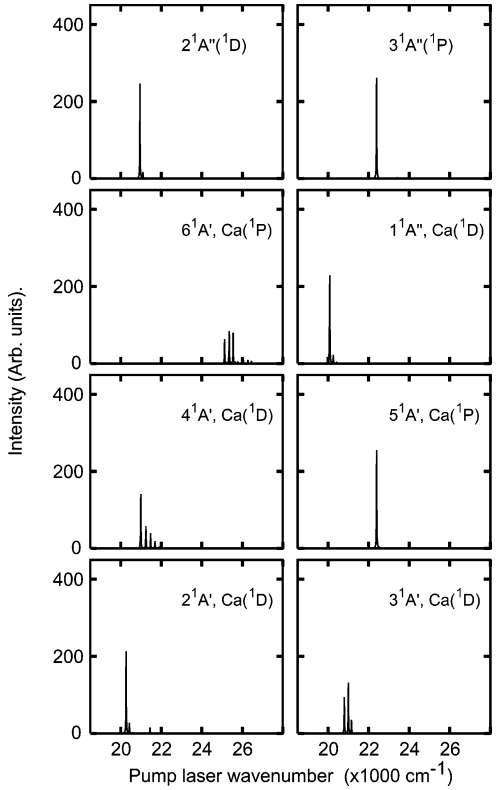

Figure 9. Absorption spectra obtained from short wave packet propagations on the different excited electronic states of Ca−F−CH_3.

electronic PES: ≈500 and ≈150 cm^{-1} for the F−X vibration and Ca−FX vibrations, respectively.

5.4. Absorption Spectrum. The individual absorption spectra obtained from the wavepacket dynamics for each final electronic state are shown in Figure 9. The zero of energy that is chosen for the PES in Figures 6 and 7 sets the energy E of the wavepacket with respect to dissociation toward the excited state of Ca corresponding to the PES under consideration (the zero point energy of CH_3F in the dissociation asymptote is not included). The energies that appear in Figure 9 refer to the excitation energy from the van der Waals well of the ground-state complex. Hence, they are deduced from E by the expression

$$h\nu = -E_b + E_{Ca^*} + E$$

where $E_b = -274$ cm^{-1} is the energy of the ground vibrational level in the ground-state PES $1^1A'$ and $E_{Ca^*} = 21\,850$ or $23\,652$ cm^{-1} is the electronic energy of Ca in the $4s3d^1D$ or $4s4p^1P$ levels, respectively (these are the experimental energies[33]) (note that E_b is not the dissociation energy of the complex, because the latter should include the zero point energy ofCH_3F).

Except for the $6^1A'$ state, all the transitions that appear in Figure 9 are located on the red side of the calcium resonance line (23 652 cm^{-1}) where the present experimental results are recorded. Hence only the $1-5\ ^1A'$ and $1-3\ ^1A''$ are relevant for the present work and are considered hereafter.

The full absorption spectrum is obtained by summation of the individual spectra of Figure 9. It is plotted in the bottom panel of Figure 10 where it is compared to the action spectrum of reaction 2 that has appeared in Figure 4a. The simulated spectrum, which extension is larger than 2000 cm^{-1} is shifted by a small amount, +175 cm^{-1}, to improve the matching between the simulation and the experiment.

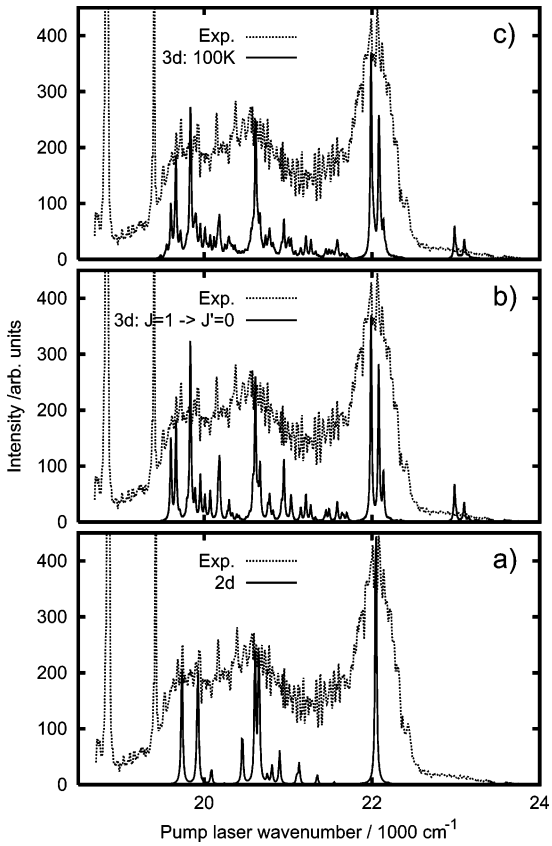

Figure 10. Comparison between the simulated absorption spectrum and the reaction action spectrum taken from Figure 4a. The theoretical spectra correspond to the 2d simulation (bottom panel), the 3d simulation only including the $J = 0 \rightarrow J' = 1$ transitions (middle panel), and a 3d spectrum obtained considering all rotational transitions up to $J = 50$ for a temperature of 100 K (top panel).

6. Discussion

6.1. Ground-State Potential. References 1 and 2 have anticipated what is confirmed in the present calculation, a reaction barrier is present along the reaction path in the ground PES. Its height is quite large, 1.1 eV with respect to the Ca + CH_3F asymptote (see Figure 8 and Table 2). It is consistent with the experimental observation that the reaction, although exothermic, is not active when ground-state Ca atoms collide with CH_3F molecules in the beam source. Hence, nonreactive Ca···FCH_3 complexes can be formed during the supersonic expansion. The relative easiness of their formation is consistent with the presence of a deep van der Waals well, deeper than 700 cm^{-1}, along the entrance channel Ca + CH_3F.

The van der Waals minimum along the Ca + CH_3F channel defines the geometry of the Ca···FCH_3 complex from which the reaction is initiated by laser excitation. The calculation results, summarized in Table 2, restricted to a linear geometry of the Ca−F−C backbone, indicate Ca−F and F−C bond lengths of 4.60 and 2.61 au, respectively, with essentially no deformation of the CH_3F molecule in the complex compared to the free molecule. These results are close to those provided by the calculations of ref 2. Nevertheless, differences exist that reflect the more elaborate level of the calculations performed in ref 2 for the ground-state PES. According to the latter calculation, the C−F bond is slightly stretched (2.70 au versus 2.61 au), the CaF distance is 4.72 au and the Ca−F−C backbone is bent by 43°. Note that the coordinate system is not the same in ref 2 and here. The equilibrium geometry with ∠Ca−*x*−C = 140° in Figure 4 of ref 2 corresponds to $\gamma = \angle$Ca−F−C = 137° in the present work, i.e., a 43° bending of the Ca−F−C backbone.

6.2. Lifetime of the Complex. The "action spectrum" shown at the bottom of Figure 4 is a very weak signal corresponding to the ionization of the Ca···FCH_3 complex in a R2PI process of the sole pump laser. Accordingly, a first photon electronically excites the complex, which survives long enough for being ionized by a second photon during the pump pulse (3 ns duration). Because a signal is observed, although quite week, the lifetime of the complex in the intermediate state should not be extremely short compared to 3 ns. However, no signal is observed when trying to detect the excited complex in a pump−probe scheme, using the probe laser, which is delayed by 5 ns with respect to the pump laser. This sets limits to the lifetime of the excited complex. A compromise between these considerations could be a lifetime in the range 50−500 ps.

6.3. Experimental Action Spectrum of the Reaction. The action spectrum of reaction 2 is assigned in section 4.3 to the smoothly structured band that appears in the top panel of Figure 4. It corresponds to a pump−probe scheme where the probe laser ionizes the product molecule CaF when electronically excited in the B $^2\Sigma^+$ or B′$^2\Delta$ states (see Figure 3. The band is extending between 420 and 535 nm. It can be understood as the superposition of three overlapping spectral features of comparable importance where substructures might be recognized within the experimental noise. The location and width of the spectral features are, 19 800 ± 200, 20 600 ± 360, and 22 100 ± 250 cm^{-1}. Likely, they find their origin in one or several absorption bands of the complex, filtered by the branching to the electronically excited reaction product. The assignment of these spectral features will be done in the next section by comparison with the calculated absorption spectrum.

The action spectrum of reaction 2 is extending much further to the red than the "action spectrum" discussed in section 6.2 when monitoring the $CaCH_3F^+$ ion. The reason is simply energetic because the R2PI detection of the complex is no longer allowed energetically when the wavelength of pump laser is tuned beyond 475 nm. In the wavelength range where the two action spectra can be compared, the resemblance between both is striking. They consist of a peak of about 13 nm full width at half-maximum, broadly peaking at 452 nm. This indicates that both spectra have a common origin. Upon electronic excitation in this energy region, the complex has the lifetime of 50−500 ps discussed in section 6.2 and goes to reaction within this time window.

A final point must be made about the possible competition between reaction and dissociation of the complex. Energy considerations show that the adiabatic dissociation channel in the singlet excited state is closed when exciting the complex within the action spectrum of the reaction shown in the top panel of Figure 4. The threshold value for dissociating the complex as Ca(4s3d ^{1}D) + CH_3F is indeed either 25 280 or 22 700 cm^{-1} whether the ground-state binding energy of the complex is set to 731 cm^{-1} as calculated in the present work or to 850 cm^{-1} as provided by the more elaborate calculation of ref 2. Both values are larger than the energy deposited in the complex after excitation in the blue wing of the action spectrum. Hence, dissociation is blocked energetically and the fate of the complex can be only reaction, energy relaxation within the singlet multiplicity or intersystem energy transfer to triplet PES's. Radiative decay that might be added to this list seems too slow to compete with these processes within the estimated lifetime of the complex, 50−500 ps.

6.4. Comparison between the Experimental Action Spectrum of the Reaction and the Calculated Absorption Spectrum. Three groups of lines can be recognized in the calculated absorption spectrum shown in Figure 10a. The first group is formed with the three lines close to 20 000 cm^{-1}. They correspond to exciting the complex to the neighboring states, $2^1A'$ and $1^1A''$. This stems from Figure 9 where absorption spectra are shown for individual electronic transitions. The second group of lines is extending between 20 500 and 21 500 cm^{-1} and corresponds to exciting the complex to the $3^1A'$, $2^1A''$, and $4^1A'$ states; finally the third group, a line close to 22 000 cm^{-1} is a superposition of transitions to the quasi degenerate states $5^1A'$ and $3^1A''$. The states involved in the two first groups of lines correlate to Ca(4s3d ^{1}D) in the entrance valley, whereas the states $5^1A'$ and $3^1A''$ correlate to Ca(4s4p ^{1}P) (see Table 1).

A striking one-to-one correspondence appears in the line locations in Figure 10a when comparing the experimental action spectrum to the calculated absorption spectrum. The three overlapping spectral features of the experimental action spectrum match the three groups of lines identified above in the calculated absorption spectrum. Hence, all the excited states of the complex seem to lead to reaction with the following assignment: (i) the red spectral feature of the action spectrum corresponds to reaction after excitation to the $2^1A'$ and $1^1A''$ states of the complex; (ii) the middle spectral features to reaction from the $3^1A'$, $4^1A'$, and $2^1A''$ states of the complex, and (iii) the blue spectral feature to reaction from $5^1A'$ and $3^1A''$.

Two observations providing information on the reaction dynamics of the system follow this assignment. First, the three spectral features in the action spectrum have roughly the same area. This implies that the product of the oscillator strength for the excitation of the complex, times the branching to the formation of electronically excited CaF is about the same after integration over the spectral feature. Second, the calculated lines have a width of about 10 cm^{-1}, whereas the spectral features in the action spectrum are much broader, 200−360 cm^{-1}. The remaining of the discussion examines the dynamical consequence of these two points.

6.5. Puzzling Dynamics in the $2^1A'$ and $1^1A''$ States. Of the two points made in the previous section, one suggests a compensation between a small oscillator strength to excite the complex and a large reaction probability of the excited complex. By focusing our attention on the excitation of the $2^1A'$ and $1^1A''$ states, we shall see here that this compensation does not result from straightforward phenomena.

The MCSCF calculation of ref 2 has provided transition dipoles, which were not reported in the paper. Those describing the $2^1A' \leftarrow 1^1A'$ and $1^1A'' \leftarrow 1^1A'$ transitions are very small because of the strong "Δ" character of the $2^1A'$ and $1^1A''$ states. These states are formed indeed from the 3d δ orbital of Ca and the Ca···FCH_3 system behave as a quasi-linear molecule. This analysis applies strictly to the 0−0 bending band of the $2^1A' \leftarrow 1^1A'$ and $1^1A'' \leftarrow 1^1A'$ transitions. Because the bending of the complex is almost doubly degenerate, the Renner−Teller effect is active and the other vibronic bands have a larger oscillator strength, as observed in the related species Ca−OCH_3, Ca−OC_2H_5, and Ca−CCH.[34] This effect may be quite large because the complexes are not very cold, ≈100 K, making the weak bending mode significantly populated.

On the other hand, Figure 8 shows that reaction barriers are predicted along all the adiabatic reaction paths. The lowest one is encountered on the curve drawn from the $2^1A'$ PES calculation but still, it cannot be overcome with the excitation energies of the blue wing of the action spectrum. Less than 23 000 cm^{-1} are deposited, whereas 23 900 cm^{-1} are needed to overcome the calculated barrier. It can be thought that the calculated barriers are lowered substantially, or even suppressed if fully optimizing the Ca−F−C backbone in the PES calculation. A qualitative study of the excited PES's has been performed in nonlinear geometry to explore this possibility. The shape of the reaction paths shown in Figure 8 is changed in the reaction side, though not on the entrance side. For example, following the curves built from the $1^1A'$ and $2^1A'$ surfaces, from the left-hand side to the right-hand side of the figure, a broad well appears in each curve at negative values of the reaction coordinate (reaction side) between −10 and −3 au. These wells describe respectively the ground and first excited state of the insertion intermediate $FCaCH_3$. Their depth is 18 000 and 11 500 cm^{-1}, with respect to the corresponding asymptotes CaF(X $^2\Sigma^+$)+CH_3 (curve $1^1A'$) and CaF(A $^2\Pi$)+CH_3 (curve $2^1A'$). Potential wells that are much shallower, are also present along the other curves (including the $1A''$ curve). In contrast, neither the depth of the van der Waals well nor the height of reaction barrier along the curves $1^1A'$, $1^1A''$, and $2^1A'$ is modified dramatically in the bent geometry. This suggests that in the ground and first excited states of Ca···FCH_3, the C−F bond has to be stretched in an endothermic way, prior Ca finds an exothermic route to the insertion or to the reaction.

At this point, we are facing the puzzling situation announced at the beginning of this section: (i) exciting the complex in the $2^1A'$ or $1^1A''$ states has a moderate oscillator strength and (ii) the reaction is blocked by a barrier. Nevertheless, a strong reactive signal is observed when the complex is excited with pump photons corresponding to the $2^1A'$, $1^1A'' \leftarrow 1^1A'$ transitions. The next two sections present explanations for this apparent contradiction by considering dynamical processes acting either simultaneously or sequentially.

6.6. Nonadiabatic Energy Transfers, Intersystem Crossings and Tunneling Reaction. From section 6.2 we know that the excited complex has a lifetime in the range 50−500 ps and elaborating on section 6.3 with the help of section 6.5 we anticipate and discuss hereafter that the following processes could act prior to the reaction: (i) nonadiabatic energy transfers from singlet PES's above $2^1A'$ down to $2^1A'$, (ii) nonadiabatic energy transfer down to $1^1A'$, and (iii) intersystem transfer from singlet to triplet PES's.

(i) Nonadiabatic Energy Transfers down to $2^1A'$. The reaction forming excited CaF is observed, irrespective of the electronic state of the complex that is excited, $2-5^1A'$ or $1-3^1A''$. The reaction barriers along the $3-5^1A'$ and $1-3^1A''$ states are much higher than that associated to the $2^1A'$ state. Hence, the system has to transfer to the $2^1A'$ surface for the reaction. However, we have seen in section 6.5 that this does not provide enough energy to overcome the reaction barrier along the $2^1A'$ surface. Hence, after transfer to this surface, the system is blocked in the van der Waals well of the $2^1A'$ surface where is oscillates. If the reaction proceeds from this surface, it has to proceed by tunneling through the reaction barrier.

The time scale for such a tunneling reaction depends on several factors: the height and width of the barrier, the vibrational constant of the oscillation in the van der Waals well, and the excess energy that is provided by the laser excitation. When standard textbook formulas of the tunneling probability are used, time scales of 1 ps, 1 ns, or 30 ns are obtained whether the excess energy corresponds to an excitation of the complex in the blue, middle, or red spectral feature of the action spectrum.

Such calculation assumes that, whatever the state that is excited by the pump laser, the system has transferred to $2^1A'$, the only excited state that could yield a significant tunneling reaction rate. Experimentally, the lifetime of the complex is estimated to 50−500 ps. Although not precluded, tunneling is unlikely, especially when the $2^1A'$ state is excited with almost no excess energy (red spectral feature in the action spectrum). The wavepacket calculation can be used in the latter case to make the estimation of the tunneling time scale more quantitative. The autocorrelation function shows a very slow decay corresponding to a lifetime of ≈ 11ns hence, confirming that the tunneling mechanism is unlikely.

(ii) Nonadiabatic Energy Transfers down to $1^1A'$. It appears in Figure 8 that a nonadiabatic transfer from the $2-5^1A'$ or $1-3^1A''$ states to the $1^1A'$ state could convert enough electronic energy into vibration of the ground-state system to overcome the reaction barrier. At the same time, this would also open the dissociation channel of the complex and both reaction and dissociation would compete. If these two processes proceed adiabatically on the ground-state PES, then ground-state products, Ca or CaF, would be formed. Electronically excited CaF is detected in the present experiment. Hence, if active this reaction mechanism should imply a late nonadiabatic back transfer to electronically excited CaF. Such a process is not excluded because the $2^1A'$ surface has likely several coupling regions with the ground-state surface $1^1A'$. However, when the system has transferred to the ground-state surface, it will evolve toward the equilibrium geometry of this surface (that shown in Figures 6 and 8) where the $1^1A'$ and $2^1A'$ surfaces are very distant. We believe that this evolution makes the back transfer to $2^1A'$ unlikely, as soon as either CH_3 (for a movement in the reaction valley) or CH_3F (for a movement in the entrance valley) has started to move away, taking away some of the excess energy. In other words, the jump down to the $1^1A'$ surface and the subsequent evolution on this surface increases tremendously the density of states that is accessible to the system. Hence, the wavepacket describing the evolution of the system will spread over a very large number of modes, which make it highly improbable to come back to the $2^1A'$ surface, where the density of states is much smaller. Of course, a full exploration of the coupling between the $1^1A'$ and $2^1A'$ surfaces would be very useful to ascertain this statement.

(iii) Intersystem Transfer from Singlet to Triplet PES's. Intersystem crossing offers an alternative reaction mechanism by giving access to reaction pathways along triplet PES's. Its time scale is consistent with the estimated lifetime of the excited complex, 50−500 ps.

The triplet PES's closest to the $2^1A'$ PES correlate with Ca(4s3d ^3D) + CH_3F in the entrance valley and to either CaF($B^2\Sigma^+$) + $CH_3(X^2A_2'')$ or CaF($B'^2\Delta$) + $CH_3(X^2A_2'')$ in the reaction valley. There is no reason to expect that the energy barriers for the reaction are dramatically different in the triplet surfaces compared to the corresponding singlet surfaces. In the entrance valley, the triplet surfaces correlating to Ca(4s3d^{3}D) + CH_3F are expected to be fairly parallel to the corresponding singlet PES's correlating toCa(4s3d^1 D) + CH_3F. Hence, the energy release corresponding to the energy transfer from the singlet surface $2^1A'$ to one of these triplet surfaces is expected to be comparable to the $^1D-^3D$ energy splitting in free Ca. This provides an additional ∼1500 cm^{-1} vibrational energy that is enough either to overcome the smallest energy barriers along the triplet surfaces or to tunnel through it. Thus, triplet surfaces offer a slow, indirect but unavoidable route for the reaction forming electronically excited CaF.

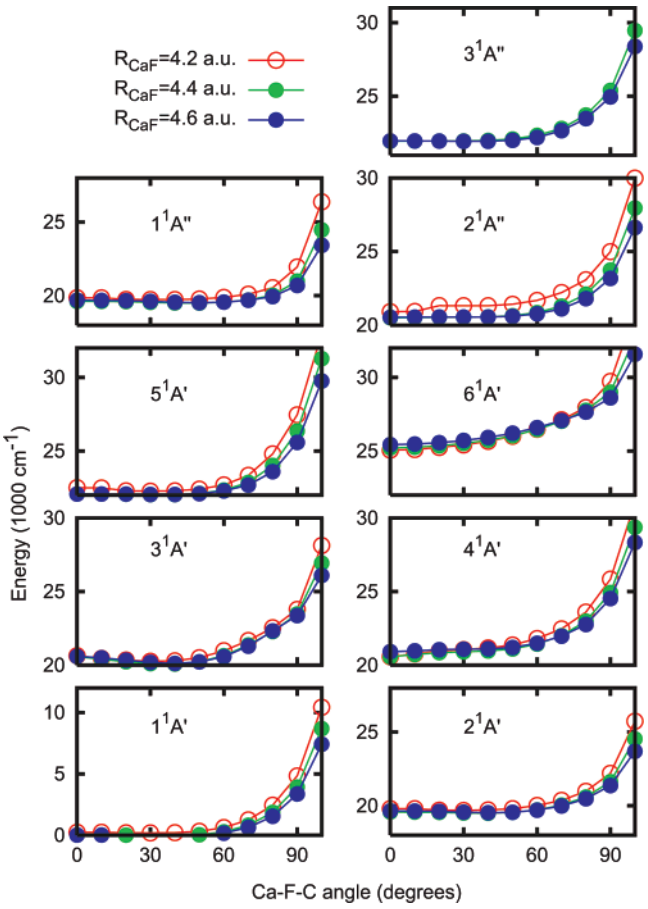

Figure 11. Dependence of Ca···FCH_3 potential energies as a function of the ∠Ca−F−C angle for several electronic states and three Ca−F distances labeled in the figure. The FCH_3 moiety is set to its equilibrium geometry as a free molecule. The zero of energy is referred to the energy of the Ca···FCH_3 ground electronic state when R_{CaF} = 4.4 au and ∠Ca−F−C = 0°.

An important point is that the reaction pathway along triplet PES's correlates with the electronically excited states of CaF, B, and B′, which are detected in the present experiment. Hence, when the reaction proceeds and reaches regions of higher and higher density of states when the system dissociates as reaction products, no back transfer to surfaces of higher electronic energy is required to reach the detected states. In contrast, such unlikely transfers needed to be invoked in the reaction pathways discussed in paragraphs (i) and (ii) above, where only singlet PES's are involved. For this reason we favor the assumption that the reaction goes along triplet PES's.

6.7. Role of the Bending. The question of bending oscillations of the Ca···FCH_3 has appeared at various points of the discussion. To make it semiquantitative, the Ca−F−C bending and the overall rotation angular momentum is included tentatively in the simulation.

The dependence of the PES's on the γ Jacobi angle is generated first using the CI-MRCI calculations described in section 3.1, but in the present case the F−C distance and the CH_3 geometry are frozen to their equilibrium values in free CH_3F and the Ca−F distance is sampled around the van der Waals well. The results are shown in Figure 11 for three values of the Ca−F distance. The curves have a similar shape. The curve corresponding to R_{CaF} = 4.2 au in the panel $3^1A''$ is not shown because of convergence problems that made it very inaccurate. As a first approximation we describe the full PES's (actually 3D-PES's) by a sum of two terms: the 2D-PES's used

elsewhere in this paper, plus the angular part obtained by a 1-dimensional spline interpolation of the points shown in Figure 11. This approximation is expected to be valid in the vicinity of the van der Waals well, which is also the Franck−Condon region for excitation of the complex from its equilibrium geometry.

The wavepacket calculations that follow the 3D-PES's calculation are similar to those presented in ref 26. Bound states on each electronic state are calculated as the product of a radial and an angular function and the transition matrix can be calculated from the transition dipole moments. It is assumed that the transition dipole moment for $A' \leftarrow A'$ transitions have *z* and *x* components of equal strength, but for $A'' \leftarrow A'$ ones they only have the *y* component. Each transition is dressed with a Lorentzian function of 10 cm^{-1} of width to be consistent with the 2D wave packet calculation.

Figure 10b displays an absorption spectrum simulated by this technique, which includes the $J' = 1 \leftarrow J'' = 0$ transitions from the ground van der Waals level of the $1^1A'$ state (*J* is the total angular momentum of the system). The three groups of lines that appeared in the 2D calculations (Figure 10a) can still be recognized. Several peaks are split, hence making each group of line broader, especially the groups corresponding to the red and middle spectral features of the action spectrum, i.e., the two groups of lines corresponding to the excitation of states correlating to Ca(4s3d ^{1}D) + CH_3F.

The top spectrum in Figure 10 shows a simulation where the transitions up to $J'' = 50$ are considered and averaged over a Boltzmann distribution at 100 K corresponding to the temperature of the complexes in the experiment. The average also includes the bending levels that are populated at this temperature. Comparing the simulated spectra in the top and middle panels of the figure, a broadening is noticeable, but not many new peaks appear. This implies that excited van der Waals levels on the ground electronic state participates very weakly, and that the observed broadening is essentially due to a larger rotational congestion at 100 K. This is especially apparent in the groups of lines below 22 000 cm^{-1}. They mimic the broad spectral features observed in the experimental spectrum. Nevertheless, the well resolved structures that appear in the calculation are hardly recognizable in the experimental action spectrum and the shape of the middle and blue spectral features in the action spectrum are not accurately reproduced. This is not surprising in fact and simply confirms the expectations drawn above that the excited system experiences nonadiabatic energy transfers within the single multiplicity and intersystem crossings to triplet PES's. These phenomena, which are not included yet in the calculation, should result into a broadening of the calculated lines.

6.8. Ca(4s3d ^{1}D) + CH_3F, CH_3Cl, CH_3Br Reactions in Full Collision. Reference 35 reports a study of the Ca(4s3d ^{1}D) + CH_3F reaction in full collisions. It aimed to study the steric effect of Ca approaching favorably the F end of CH_3F or unfavorably the other end. A series of semiclassical calculations were performed to account for these experiments. They assumed a cone of acceptance for the reaction making it impossible when Ca collides the unfavorable side of CH_3F and possible with no barrier when Ca collides the F atom.[36−38] In the latter case, the reaction would be direct. These calculations reproduced qualitatively the experimental results but did not reach a quantitative agreement although the reaction model contained adjustable parameters.

The potential calculations reported above address specifically the favorable approach of Ca from CH_3F because the PES's document the collinear approach Ca−F−C. As already discussed, all the states correlating to Ca(4s3d ^{1}D) + CH_3F at infinite separation between Ca and CH_3F present a barrier to the reaction and the present experiment reveals that the time scale of the reaction is a fairly slow, 50−500 ps. The corresponding undirect reaction mechanism discussed in the present work could not be anticipated in ref 35. Its role in the steric effect experiments is discussed now. The results of Table 2 show that 0.17 eV are needed to overcome the energy barrier along the $2^1A'$ surface. Figure 9 in ref 35 shows the steric effect in the Ca(4s3d ^{1}D) + CH_3F reaction as a function of the collision energy. Strikingly, the data can be read differently than suggested by the fit shown in the figure: the steric effect is small and constant up to 0.22 eV collision energy, then it increases steadily. This might reflect a change in the reaction mechanism whether the collision energy is smaller or larger than the reaction barrier that is probably orientation dependent as suggested in ref 35. Small collision energy would lead to the indirect reaction mechanism discussed in the present work whereas an orientation dependent reaction mechanism would be experienced at collisions energies above 0.22 eV.

Finally, Dagdigian an co-workers reported chemiluminescent cross sections for the reaction of Ca(4s4p $^3P_0$) and Ca(4s3d $^1D_2$) with CH_3Cl and CH_3Br.[39] The cross section with Ca(4s3d $^1D_2$) is more than an order of magnitude larger than that with Ca(4s4p $^3P_0$) (see Table 2 in ref 39). Given the similarity between the three molecules, CH_3Cl, CH_3Br and CH_3F, the reaction mechanism with CH_3Cl and CH_3Br is likely to proceed along the same lines as that discussed in the present work with CH_3F. Actually, the experimental observation of Dagdigian fits well with the paragraph (iii) in section 6.6 of the present discussion. We indeed infer in this paragraph that the reaction forming electronically excited CaF does not proceed directly from the $2^1A'$ PES (that correlates to Ca(4s3d ^{1}D) + CH_3F) because it is blocked by a reaction barrier, but from a triplet surface underneath the $2^1A'$ PES, the energy difference between the two surfaces giving a sufficient excess energy to the system to overcome to tunnel through a barrier that likely exists along the triplet surface also. The large chemiluminescent cross sections measured for Ca(4s3d $^1D_2$) in the work by Dagdigian could be due to a similar reaction mechanism, whereas the very small cross section measured for Ca(4s4p $^3P_0$) would result from the energy barrier in the triplet energy surface correlating to Ca(4s4p $^3P_0$) + CH_3Cl, and CH_3Br, too large to be overcome by the thermal collision energy in the experiment.[39] This new perspective shed a different lighting, impossible to give without the present potential energy calculations, on the interpretation of ref 39, which merely discussed the branching ratio to the chemiluminescence rather than the full reaction cross section.

7. Conclusion

The present paper, the third of the series, examines the photoinduced reaction both experimentally and theoretically.

$$Ca\cdots CH_3F \xrightarrow{h\nu \in [18\,000-24\,000\ cm^{-1}]} CaF(\geq B^2\Sigma^+) + CH_3$$

Experimentally, 1:1 Ca···CH_3F complexes are formed in the pulsed supersonic expansion of a He/Ca/CH_3F mixture and a pump laser tuned in the range 18 000−24 000 cm^{-1} turns on the reaction. The detection allows us to monitor the excited reaction product (CaF in the $B^2\Sigma^+$ state or above) as a function of the wavenumber of the pump laser. The excitation range that is chosen corresponds to the band A of the preliminary action

spectrum that appeared in paper II of this series. The band extends between 19 000 and 23 000 cm^{-1}. The present work shows that it is structured into three broad overlapping spectral features. The band of lowest energy is assigned to the excitation of the complex to the $2^1A'$ and $1A''$ state and subsequent reaction; the spectral feature of higher energy corresponds to excitation and reaction from the 3 other states, $3^1A'$, $2^1A''$, $4^1A'$ that correlated to Ca($4s3d^1$ D) + CH_3F at infinite separation between Ca and CH_3F; finally the spectral feature of larger energy corresponds to the excitation of two states correlating to Ca($4s4p\ ^1P$) + CH_3F. In this paper, attention has focused on the first two spectral features and their interpretation in terms of reaction mechanism with the help of the calculation. The experiment also allows an estimation of the lifetime of the excited complex, 50−500 ps.

On the theoretical side, the Ca···CH_3F complexes are described by 2D-PES's where the Ca−F−C backbone is considered as linear and the Ca−F and F−C distances varied systematically. A 2D grid is built, exploring two rearrangement channels, dissociation of the complex as Ca + CH_3F and the reaction CaF + CH_3. The PES calculations are performed at the CI-MRCI level and document all the excited states of the complex correlating to the $4s^2\ ^1S$, $4s3d\ ^1D$, and $4s4p\ ^1P$ levels of Ca in the entrance channel. Then, wavepacket calculations on the 2D grid allows one to simulate the absorption spectrum of the complex, in an approximation where the various electronic states of the complex are not coupled together. The calculated absorption spectrum is formed of three groups of lines that matches the three spectral features of the experimental action spectrum. Actually the assignment of the spectral features recalled above stems from the calculated absorption spectrum.

Importantly, the PES calculations show that whatever the excited level of the complex that is considered, the reaction has to proceed through energy barriers. The lowest barrier is encountered along the $2^1A'$ surface to which the 4s3d δ orbital of calcium contribute importantly. An analogy with the reactivity of transition metals could be called for. Nevertheless, this lowest barrier is still quite high and the reaction mechanism through this state should be tunneling, an unlikely process when the laser excitation does not provide a large excess energy above the $2^1A'$ state. Another reaction mechanism implying a nonadiabatic energy transfer to the ground-state PES followed by a back transfer to an electronically excited PES is also considered. Finally a reaction mechanism implying an intersystem crossing to a triplet PES is preferred.

In conclusion, the reaction mechanism following the local excitation $4s3d\ ^1D \leftarrow 4s^2\ ^1S$ in the Ca···CH_3F complex is far from direct. It involves a series of nonadiabatic couplings that transfer the system to the lowest excited singlet surface $2^1A'$ when the excitation is performed to a higher state. The excess energy provided to the system might be large enough to stimulate a tunneling reaction through the barrier in the $2^1A'$ state. However, an even more indirect mechanism seems more likely, especially when the pump laser populates the $2^1A'$ with no excess energy. This mechanism goes through a transfer to a triplet PES. Finally, a Renner−Teller like effect implying the bending of the complex seems necessary to account for the spectrally extended reactive signal observed experimentally. In this context, would be highly necessary to probe the evolution of the system in the real time to determine its lifetime in several types of excited PES's.

Acknowledgment. Partial support is acknowledged from the Spanish-French bilateral grant Picasso-no 09252TM and from the European Community through the PICNIC network (Product Imaging and Correlation: Non-adiabatic Interactions in Chemistry) under contract number HPRN-CT-2002-00183.

References and Notes

(1) Gaveau, M. A.; Gloaguen, E.; Fournier, P. R.; Mestdagh, J. M. *J. Phys. Chem. A* **2005**, *109*, 9494.
(2) Mestdagh, J. M.; Spiegelman, F.; Gloaguen, E.; Collier, M.; Lepetit, F.; Gaveau, M. A.; Sanz, C. S.; Soep, B. *J. Phys. Chem. A* **2006**, *110*, 7355.
(3) Mestdagh, J. M.; Soep, B.; Gaveau, M. A.; Visticot, J. P. *Int. Rev. Phys. Chem.* **2003**, *22*, 285.
(4) Hudson, A. J.; Oh, H. B.; Polanyi, J. C.; Piecuch, P. *J. Chem. Phys.* **2000**, *113*, 9897.
(5) Hudson, A. J.; Naumkin, F. Y.; Oh, H. B.; Polanyi, J. C.; Raspopov, S. A. *Faraday Discuss.* **2001**, *118*, 191.
(6) Skowronek, S.; Pereira, R.; González Ureña, A. *J. Chem. Phys.* **1997**, *107*, 1668.
(7) Skowronek, S.; Pereira, R.; González Ureña, A. *J. Phys. Chem. A* **1997**, *101*, 7468.
(8) Skowronek, S.; Jiménez, J. B.; González Ureña, A. *J. Chem. Phys.* **1999**, *111*, 460.
(9) Farmanara, P.; Stert, V.; Radloff, W.; Skowronek, S.; González Ureña, A. *Chem. Phys. Lett.* **1999**, *304*, 127.
(10) Stert, V.; Farmanara, P.; Radloff, W.; Noack, F.; Skowronek, S.; Jiménez, J.; González Ureña, A. *Phys. Rev. A* **1999**, *59*, R1727.
(11) Skowronek, S.; González Ureña, A. *Prog. React. Kinet. Mech.* **1999**, *24*, 101.
(12) Skowronek, S.; Jiménez, J. B.; González Ureña, A. *Chem. Phys. Lett.* **1999**, *303*, 275.
(13) Stert, V.; Farmanara, P.; Ritze, H.-H.; Radloff, W.; Gonzalez-Ureña, A. *Chem. Phys. Lett.* **2001**, *337*, 299.
(14) Skowronek, S.; González Ureña, A. The (Ba···FCH3)* photofragmentation channels: Dynamics of the laser induced intracluster (Ba···FCH_3)* → BaF* + CH_3 and Ba* + FCH_3 reaction. *Atomic and Molecular Beams: The State of the Art 2000*; Springer-Verlag: Berlin, 2001; pp 353−366.
(15) Gasmi, K.; Skowronek, S.; González Ureña, A. *Chem. Phys. Lett.* **2003**, *376*, 324.
(16) Gasmi, K.; Skowronek, S.; Urena, A. G. *Eur. Phys. J. D* **2005**, *33*, 399.
(17) Stert, V.; Ritze, H. H.; Farmanara, P.; Radloff, W. *Phys. Chem. Chem. Phys.* **2001**, *3*, 3939.
(18) Stert, V.; Ritze, H. H.; Radloff, W.; Gasmi, K.; Gonzalez-Ureña, A. *Chem. Phys. Lett.* **2002**, *355*, 449.
(19) Stert, V.; Ritze, H. H.; Radloff, W. *Chem. Phys. Lett.* **2002**, *354*, 269.
(20) Lippert, H.; Manz, J.; Oppel, M.; Paramonov, G. K.; Radloff, W.; Ritze, H. H.; Stert, V. *Phys. Chem. Chem. Phys.* **2004**, *6*, 4283.
(21) Lippert, H.; Manz, J.; Oppel, M.; Paramonov, G. K.; Radloff, W.; Ritze, H. H.; Stert, V. *Phys. Chem. Chem. Phys.* **2004**, *6*, 5086.
(22) Werner, H.-J.; Knowles, P. J. MOLPRO a package of ab initio programs, version 2005, http://www.molpro.net 2005.
(23) Childs, W. J.; Goodman, L. S.; Nielsen, U.; Pfeufer, V. *J. Chem. Phys.* **1984**, *80*, 2283.
(24) Press, W. H.; Teukolsky, S. A.; Vetterling, W. T.; Flannery, B. P. *Numerical Recipies in C - The art of scientific computing*, 2nd ed.; Cambridge University Press: Cambridge, U.K., 1997.
(25) Aguado, A.; Paniagua, M.; Lara, M.; Roncero, O. *J. Chem. Phys.* **1997**, *107*, 10085.
(26) Aguado, A.; Paniagua, M.; Sanz, C.; Roncero, O. *J. Chem. Phys.* **2003**, *119*, 10088.
(27) Paniagua, M.; Aguado, A.; Lara, M.; Roncero, O. *J. Chem. Phys.* **1999**, *111*, 6712.
(28) Sanz, C.; van der Avoird, A.; Roncero, O. *J. Chem. Phys.* **2005**, *123*.
(29) Harvey, J. N.; Schroder, D.; Koch, W.; Danovich, D.; Shaik, S.; Schwarz, H. *Chem. Phys. Lett.* **1997**, *278*, 391.
(30) Dulick, M.; Bernath, P. F.; Field, R. W. *Can. J. Phys.* **1980**, *58*, 703.
(31) Karny; Zare, R. N. *J. Chem. Phys.* **1978**, *68*, 3360.
(32) Weast, R. C.; Astle, M. J.; Beyer, W. H. *Handbook of Chemistry and Physics*, 65th ed.; CRC: Boca Raton, FL, 1984; 1984−1985.
(33) Sugar, J.; Corliss, C. *J. Phys. Chem. Ref. Data* **1979**, *8*, 865.
(34) Elhanine, M.; Lawruszczuk, R.; Soep, B. *Chem. Phys. Lett.* **1998**, *288*, 785.
(35) Janssen, M. H. M.; Parker, D. H.; Stolte, S. *J. Phys. Chem.* **1991**, *95*, 8142.
(36) Meijer, A.; Groenenboom, G. C.; Van der Avoird, A. *J. Chem. Phys.* **1994**, *101*, 7603.

(37) Meijer, A.; Groenenboom, G. C.; van der Avoird, A. *J. Chem. Phys.* **1996**, *105*, 2247.

(38) Meijer, A.; Groenenboom, G. C.; van der Avoird, A. *J. Phys. Chem.* **1996**, *100*, 16072.

(39) Furio, N.; Campbell, M. L.; Dagdigian, P. J. *J. Chem. Phys.* **1986**, *84*, 4332.

(40) Bernath, P. F.; Field, R. W. *J. Mol. Spectrosc.* **1980**, *82*, 339.

(41) Verges, J.; Effantin, C.; Bernard, A.; Topouzkhanian, A.; Allouche, A. R.; d'Incan, J.; Barrow, R. F. *J. Phys. B* **1993**, *26*, 279.

(42) Gittins, C. M.; Harris, N. A.; Field, R. W.; Verges, J.; Effantin, C.; Bernard, A.; Dincan, J.; Ernst, W. E.; Bundgen, P.; Engels, B. *J. Mol. Spectrosc.* **1993**, *161*, 303.

(43) Moore, C. E. *Atomic Energy Levels, Circular 467, Vol II*; NBS, U.S. Department of Commerce, 1952.

(44) Huber, K. P.; Herzberg, G. *Molecular Spectra and Molecular Structure. IV. Constants of Diatomic Molecules*; van Nostrand: New York, 1979.